Ninth International Conference on Computational Fluid Dynamics (ICCFD9), İstanbul, Turkey, July 11-15, 2016

ICCFD9-299

Three Dimensional Hypersonic Flow Analysis Around a Re-entry Vehicle Using Navier-Stokes Equations

Muharrem Özgün [1] , Assoc.Prof.Dr. Sinan Eyi [2]

[1]Middle East Technical University, Department of Aerospace Engineering, Ankara, 06800, Turkey
[2]Middle East Technical University, Department of Aerospace Engineering, Ankara, 06800, Turkey

Corresponding author: muharrem.ozgun@metu.edu.tr

Abstract: The purpose of this study is to develop an accurate and efficient CFD code that can be used in hypersonic flows. The flow analysis is based on the three dimensional Navier-Stokes equations. These equations are solved by using Newton/Newton-Gmres method. The analytical method is used to calculate the Jacobian matrix. Flow parameters and convective heat transfer are analyzed on Apollo AS-202 Command Module. Also, algebraic Baldwin-Lomax turbulence model and one-equation Spalart-Allmaras turbulence model is used to analyze hypersonic turbulent flow.

Keywords: Computational Fluid Dynamics (CFD), Hypersonic Flow, Turbulence Modeling, Newton/Newton-Gmres Method

1 Introduction

HYPERSONIC flow became a popular research area about 60 years ago after the military and aerospace industries recognized the importance of the field for various interests. The computational fluid dynamics (CFD) certainly was one of the key points in the success of many past space programs. Design engineers should use the best possible CFD tools for lasting development and this is important for success of the aerospace industry. Two different research fields have gained importance within the CFD community over time. One of them is the advancement of upwind schemes, which focuses especially on the mathematical point of view, and the other one is turbulence modeling. The turbulence is one of the most complex issues of classical physics, and it is also a special field of hypersonic.[1] Turbulence modeling plays a significant role in computations for hypersonic flow. Because turbulent flows are present in most of the hypersonic applications, it is often essential to use a turbulence model while modeling the flow. [2].

The hypersonic conditions are difficult to produce in an experimental facility. The cost of experiments of hypersonic flows is higher than low speed flows. Because flight conditions include immense amount of energy and the number of facilities that perform such experiments is not so much. CFD can reduce the number of experiments and it has been used as a design tool of entry capsules in the past two decades. More physical processes can be simulated with the increasing in computing power.[3] One of the critical problems that is faced at designing a reentry vehicle is the exact definition of high convective heat fluxes (aerodynamic heating) to the vehicle surface during hypersonic flight. Analysis of parameters of flow and heat transfer of a reentry vehicle may be made with the numerical integration of the Navier-Stokes equations in a dense atmosphere, where the assumption of continuity of gas medium is true. While the complexity of problems are increasing, comparison of computed results with experimental data carries great importance and success of these computed results is related with employed physical models and numerical techniques. [4]

Turbulence is important to determine the aerodynamic forces and heating for hypersonic vehicles. However, obtaining experimental data is difficult for turbulence model validation. There are only few flight tests in the literature, and these tests generally don't provide enough data. There are a number of ground-based wind tunnel hypersonic flow tests on small scaled geometries. These tests generally provide much more data relatively. However, the hypersonic ground tests commonly do not match the same total enthalpy and low free stream turbulence due to the very high velocities. Hence the verification of turbulence models with wind tunnel data generally includes extrapolation to flight enthalpies. Because of these difficulties in obtaining validation data, designers relies on computational fluid dynamics and the models for important issues such as turbulence, chemistry, ablation, etc. [5]

The models we use are algebraic Baldwin-Lomax and one-equation Spalart-Allmaras turbulence models. Baldwin-Lomax and Spalart-Allmaras turbulence models are used to model turbulent flow. Baldwin-Lomax model is an algebraic turbulence model and a form of the outer eddy viscosity that did not need knowledge of the conditions at the edge of the boundary layer was developed. [6] Spalart-Allmaras model is basically a transport equation for the eddy viscosity. It has proven to be numerically robust model, and generally gives good results for a wide variety of flows. [7]

2 Problem Statement

One of the objectives of this study is to develop a reliable and robust analysis code for hypersonic flows. The flow analysis is based on the axisymmetric Navier-Stokes equations. These equations are solved simultaneously by using Newton/Newton-Gmres method. Newton's method needs the Jacobian matrix which is the derivative of a residual vector with respect to a flow variable vector. In this study, analytical differentiation is used to evaluate the Jacobian matrix. The sparse Jacobian matrix is LU factorized and the solution is executed by using UMFPACK sparse matrix solver. Numerical integration of the Navier-Stokes equations is used for analyzing flow parameters and convective heat transfer. Lastly, the turbulence effects are examined in hypersonic flow. Three dimensional, compressible and steady-state Navier-Stokes equations can be written in generalized coordinate system as shown below.

$$\hat{R}(\hat{\mathrm{W}}) = \frac{\partial\left[\hat{F}(\hat{\mathrm{W}}) - \hat{F}_v(\hat{\mathrm{W}})\right]}{\partial\xi} + \frac{\partial\left[\hat{G}(\hat{\mathrm{W}}) - \hat{G}_v(\hat{\mathrm{W}})\right]}{\partial\eta} + \frac{\partial\left[\hat{H}(\hat{\mathrm{W}}) - \hat{H}_v(\hat{\mathrm{W}})\right]}{\partial\zeta} = 0 \tag{1}$$

R is defined as residual vector. Flow variable vector,

$$\hat{\underset{\sim}{W}} = \frac{1}{J}\begin{bmatrix} \rho \\ \rho u \\ \rho v \\ \rho w \\ \rho e_t \end{bmatrix} \tag{2}$$

Inviscid flux vectors,

$$\hat{F} = \frac{1}{J}\begin{bmatrix} \rho U \\ \rho u U + \xi_x p \\ \rho v U + \xi_y p \\ \rho w U + \xi_z p \\ (\rho e_t + p)U \end{bmatrix}, \quad \hat{G} = \frac{1}{J}\begin{bmatrix} \rho V \\ \rho u V + \eta_x p \\ \rho v V + \eta_y p \\ \rho w V + \eta_z p \\ (\rho e_t + p)V \end{bmatrix}, \quad \hat{H} = \frac{1}{J}\begin{bmatrix} \rho W \\ \rho u W + \zeta_x p \\ \rho v W + \zeta_y p \\ \rho w W + \zeta_z p \\ (\rho e_t + p)W \end{bmatrix} \tag{3}$$

Jacobian matrix that is used for coordinate transformation,

$$J = \frac{\partial(\xi,\eta,\zeta)}{\partial(x,y,z)} \tag{4}$$

are defined as shown above. Here, ρ is density, u, v and w are velocity components, p is pressure, e_t is total energy in per unit volume, U, V and W *are* contravariant velocity components. Contravariant velocity components is defined as shown below.

$$U = \xi_x u + \xi_y v + \xi_z u\,, \quad V = \eta_x u + \eta_y v + \eta_z u\,, \quad W = \zeta_x u + \zeta_y v + \zeta_z u \tag{5}$$

Equations can be written for viscous flux vectors as below.

$$\hat{F}_v = \frac{1}{J}\begin{bmatrix} 0 \\ \xi_x\tau_{xx} + \xi_y\tau_{xy} + \xi_z\tau_{xz} \\ \xi_x\tau_{xy} + \xi_y\tau_{yy} + \xi_z\tau_{yz} \\ \xi_x\tau_{xx} + \xi_y\tau_{yz} + \xi_z\tau_{zz} \\ \xi_x b_x + \xi_y b_y + \xi_z b_z \end{bmatrix},\quad \hat{G}_v = \frac{1}{J}\begin{bmatrix} 0 \\ \eta_x\tau_{xx} + \eta_y\tau_{xy} + \eta_z\tau_{xz} \\ \eta_x\tau_{xy} + \eta_y\tau_{yy} + \eta_z\tau_{yz} \\ \eta_x\tau_{xx} + \eta_y\tau_{yz} + \eta_z\tau_{zz} \\ \eta_x b_x + \eta_y b_y + \eta_z b_z \end{bmatrix},\quad \hat{H}_v = \frac{1}{J}\begin{bmatrix} 0 \\ \zeta_x\tau_{xx} + \zeta_y\tau_{xy} + \zeta_z\tau_{xz} \\ \zeta_x\tau_{xy} + \zeta_y\tau_{yy} + \zeta_z\tau_{yz} \\ \zeta_x\tau_{xx} + \zeta_y\tau_{yz} + \zeta_z\tau_{zz} \\ \zeta_x b_x + \zeta_y b_y + \zeta_z b_z \end{bmatrix} \tag{6}$$

Here, shear stress,

$$\tau_{x_i x_j} = \frac{M}{\mathrm{Re}}\left[\mu\left(\frac{\partial u_i}{\partial x_j} + \frac{\partial u_j}{\partial x_i}\right) + \lambda\frac{\partial u_k}{\partial x_k}\delta_{ij}\right] \tag{7}$$

$$b_{x_i} = u_j\tau_{x_i x_j} - \dot{q}_{x_i} \tag{8}$$

heat flux,

$$\dot{q}_{x_i} = -\left[\frac{M\mu}{\mathrm{RePr}(\gamma-1)}\right]\frac{\partial a^2}{\partial x_i} \tag{9}$$

is defined as shown. In equations above M, Re and Pr parameters show Mach, Reynolds and Prandtl numbers in order. Pressure value is obtained by using ideal gas equations.

$$p = -(\gamma-1)\left[e_t - \frac{\rho}{2}\left(u^2 + v^2 + w^2\right)\right] \tag{10}$$

In this study, AS-202 module of Apollo reentry vehicle is taken as model and shown in figure-1.

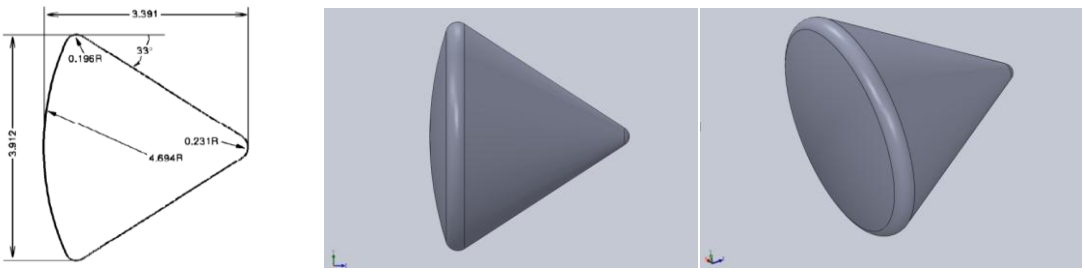

Figure 1: Dimension and solid model of Apollo AS-202 Command Module

Generated grid to analyze flow for Apollo AS-202 Command Module is seen below. The grid has half domain because of the code is axisymmetrical.

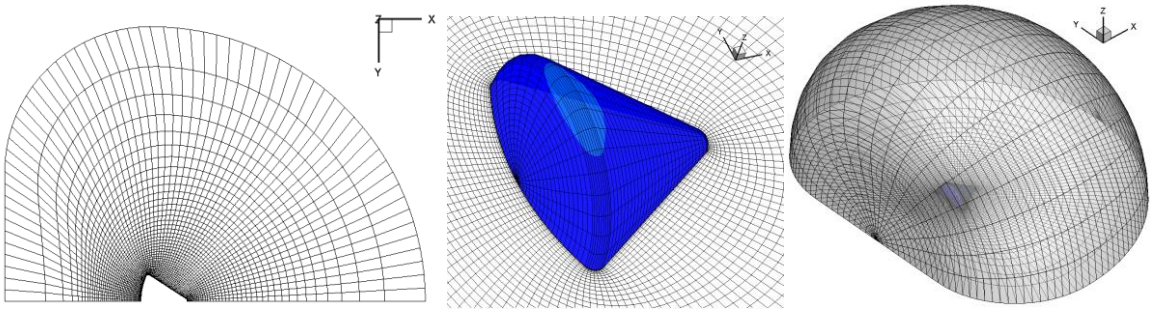

Figure-2: Grid for Apollo AS-202 Command Module

Hypersonic solver is also ran for 'Atmospheric Reentry Demonstrator (ARD)' geometry which is made by European Space Agency (ESA) for first re-entry mission. Geometry of ARD [8] and three dimensional grid of it can bee seen below.

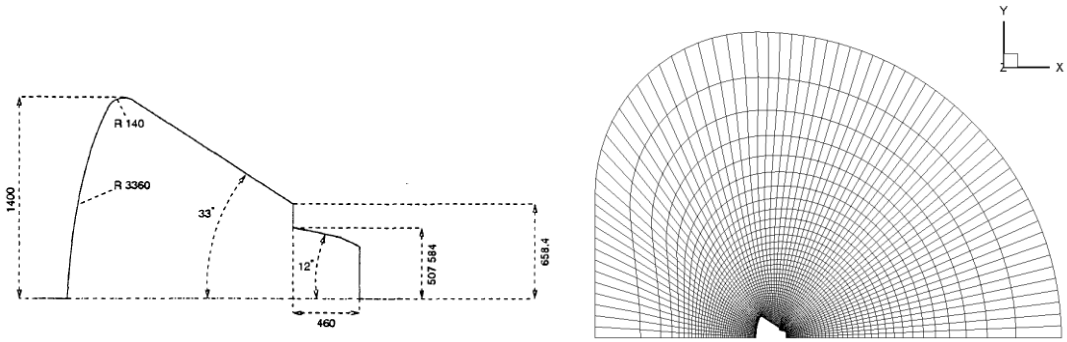

Figure 3: Geometry of ARD and 2 dimensional view of its grid.

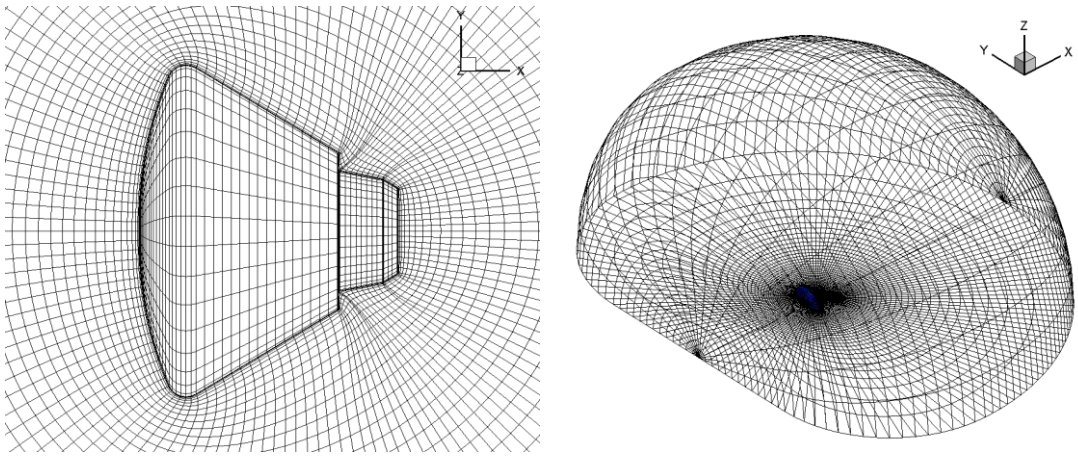

Figure 4: Grid distribution and 3-D view of grid on ARD (72x48x18)

The system of non-linear discretized governing equations can be written in the form:

$$\hat{R}(\hat{W}) = 0 \tag{11}$$

where $\hat{R}$ is the residual vector and is defined as

$$\hat{R}(\hat{W}) = \frac{\partial \hat{F}(\hat{W})}{\partial \xi} + \frac{\partial \hat{G}(\hat{W})}{\partial \eta} + \frac{\partial \hat{H}(\hat{W})}{\partial \zeta} \tag{12}$$

Expanding $R(\hat{W})$ in a Taylor series about $(n)^{th}$ iteration and discarding high order (or nonlinear) terms yields :

$$\hat{R}^{n+1}(\hat{W}) = \hat{R}^{n}(\hat{W}) + \left(\frac{\partial \hat{R}}{\partial \hat{W}}\right)^{n} \Delta \hat{W}^{n} \tag{13}$$

where $\frac{\partial \hat{R}}{\partial \hat{W}}$ is the Jacobian matrix. Solving above equation for $\hat{R}^{n+1}(\hat{W}) = 0$ formulates Newton's method as:

$$\left(\frac{\partial \hat{R}}{\partial \hat{W}}\right)^{n} \Delta \hat{W}^{n} = -R(\hat{W}^{n}) \tag{14}$$

The new values of flow variable vector $\hat{W}$ at the $(n+1)^{th}$ iteration can be calculated as:

$$\hat{W}^{n+1} = \hat{W}^{n} + \Delta \hat{W}^{n} \tag{15}$$

In the solution of Euler equations with Newton's method, the evaluation of the flux Jacobian matrix is needed. The entries of Jacobian matrix are the derivatives of the residual vector with respect to the flow variables vector. In the calculation of these derivatives a finite difference method or analytical derivation method can be used, and the resulting matrices are called numerical or analytical Jacobians, respectively.

3 Results

In figure-5, computational normalized pressure values are compared with experimental values along half nose of body when Mach number is 10.18 and angle of attack is 0°. Here, S is length of nose surface and R_b is body radius.[9] As it is seen in figure, computational result is verified with the experiment.

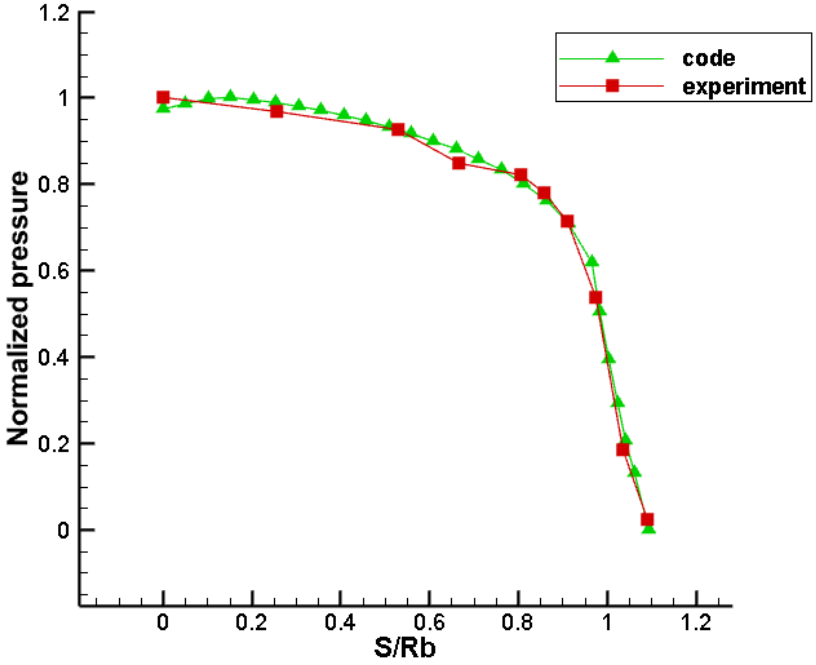

Figure 5: Comparison of the computational and experimental normalized pressure values along the body nose for the Apollo Command Module (Mach number = 10.18, flow angle = 0°)

In figure-6, computational normalized heat flux values are compared with experimental values along half nose of body when Mach number is 10.18 and angle of attack is 0°. Here, it can be seen that computational results don't match well with the experimental results and study on verification of code continues.

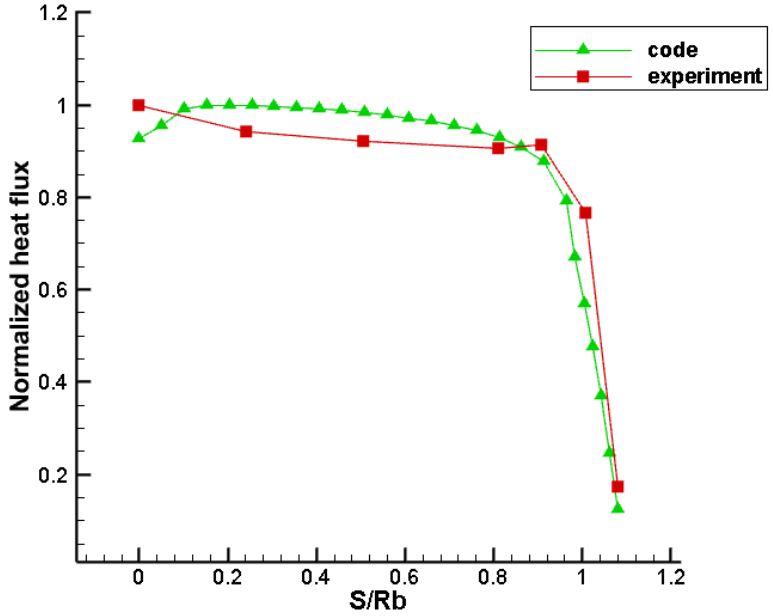

Figure 6: Comparison of the computational and experimental normalized heat flux values along the body nose for the Apollo Command Module (Mach number = 10.18, flow angle = 0°)

The Baldwin-Lomax turbulence model was implemented to the code and flow is examined when Mach number is 10 and angle between flow direction and x-axis is -30°. Mach number and pressure distributions around Apollo are seen in figure-7.

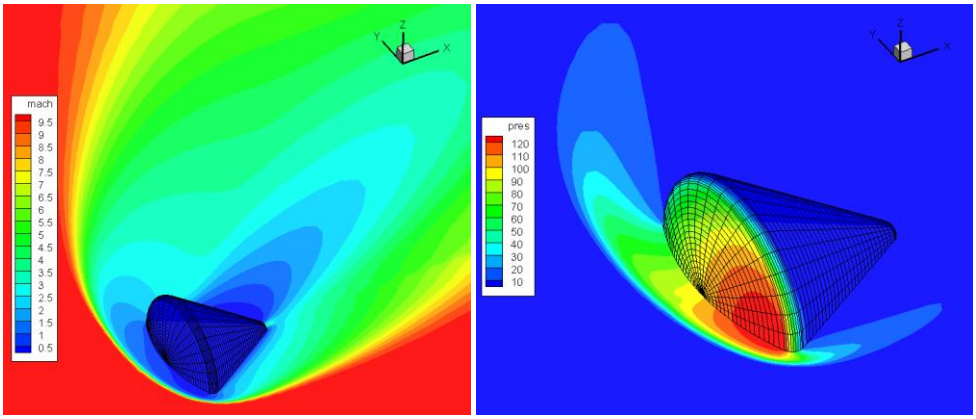

Figure 7: Mach number and pressure distributions around Apollo AS-202
(Mach number = 10, flow angle= -30°)

Density and entropy distributions around Apollo AS-202 can be seen below.

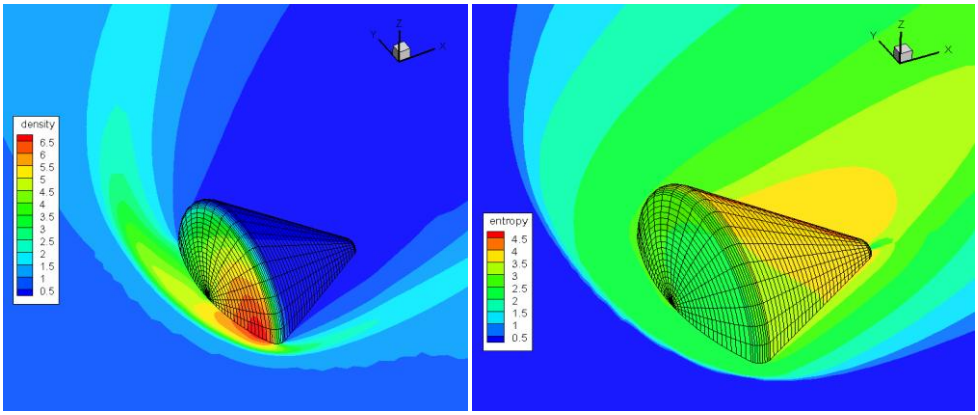

Figure 8: Density and entropy distributions around Apollo AS-202
(Mach number = 10, flow angle= -30°)

Numerical values on figures are normalized. In figure-9, taking account of real values, it is understood that the maximum temperature on nose region is very high from what they should be. The reason for that is using ideal gas equations and not to be included chemical reaction effects in the code.

The temperature distributions and velocity vectors around vehicle are seen in figure-9.

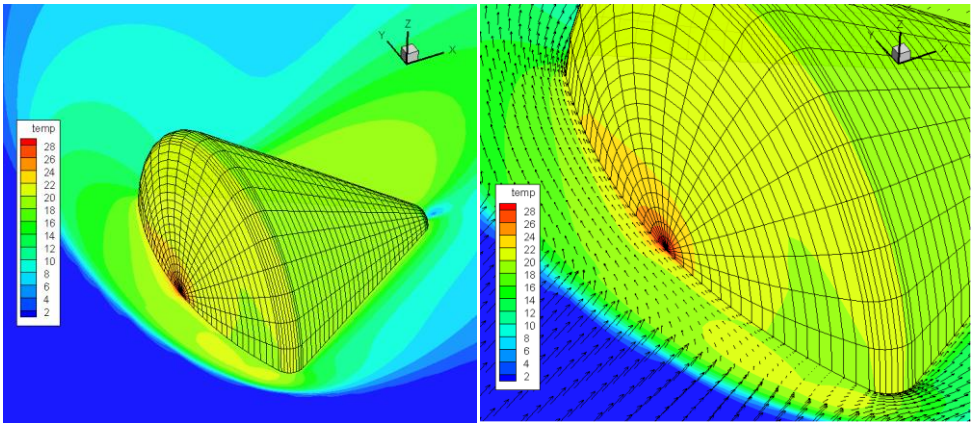

Figure 9: Temperature distributions and velocity vectors around Apollo AS-202
(Mach number = 10, flow angle= -30°)

Here, a high temperature region on the vehicle attracts attention and it is thought that the reason is occurring of stagnation point at that region. Additionally, it is noticed that velocity vectors are distributed properly with physics of boundary layer.

The results of flow analysis which Mach number is 10.18 and angle between flow direction and x-axis is 0° are shown in figure-10,11 and 12.

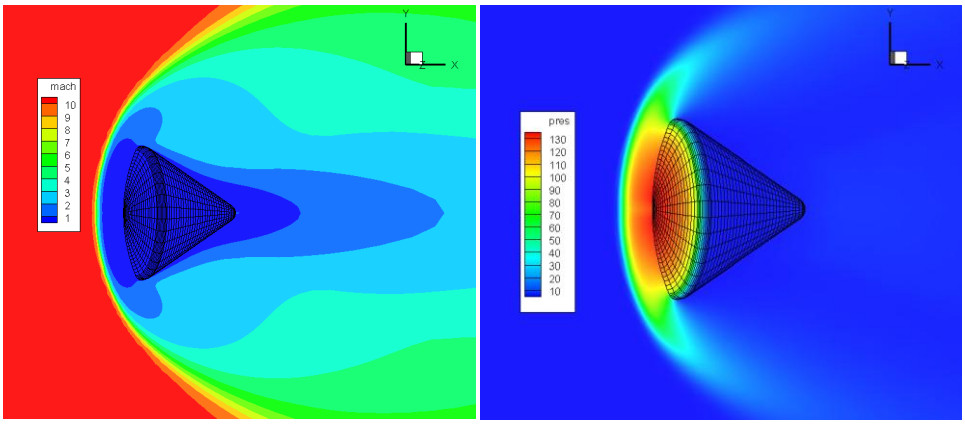

Figure 10: Mach number and pressure distributions around Apollo AS-202
(Mach number = 10.18, flow angle= 0°)

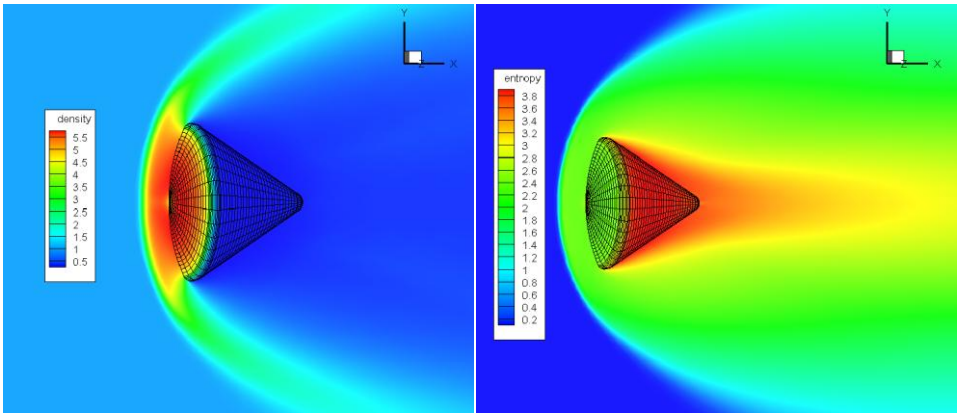

Figure 11: Density and entropy distributions around Apollo AS-202
(Mach number = 10.18, flow angle= 0°)

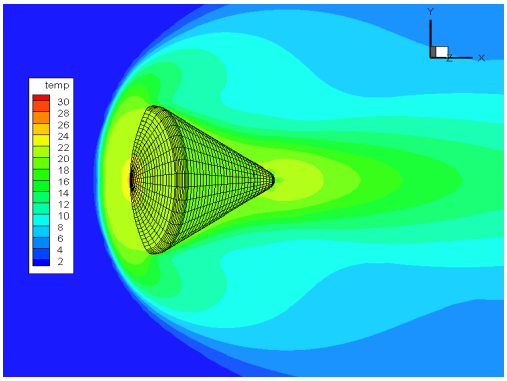

Figure 12: Temperature distributions around Apollo AS-202
(Mach number = 10.18, flow angle= 0°)

The Baldwin-Lomax turbulence model was implemented to the code and flow around ARD vehicle is examined when Mach number is 10 and angle between flow direction and x-axis is -20°. Some obtained results are seen in figure-13,14 and 15. Numerical values on figures are normalized.

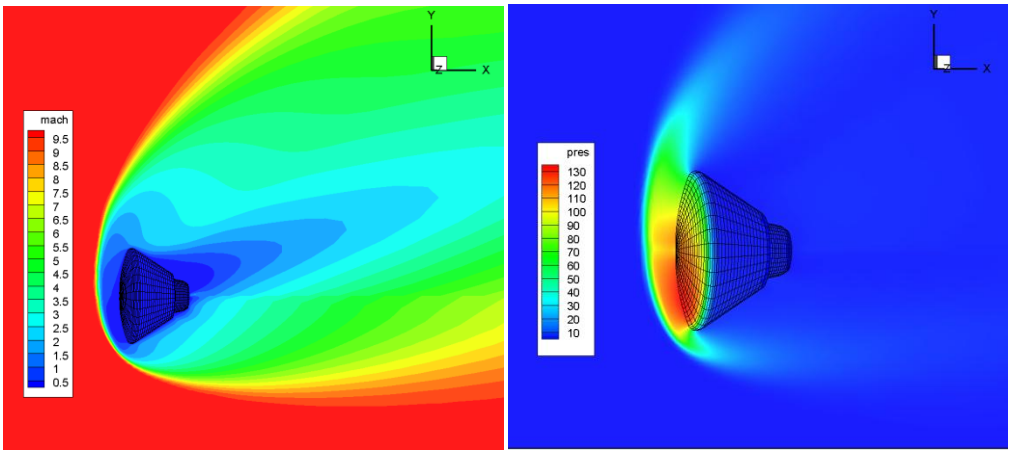

Figure 13: Mach number and pressure distributions around ARD
(Mach number=10, flow angle= -20°)

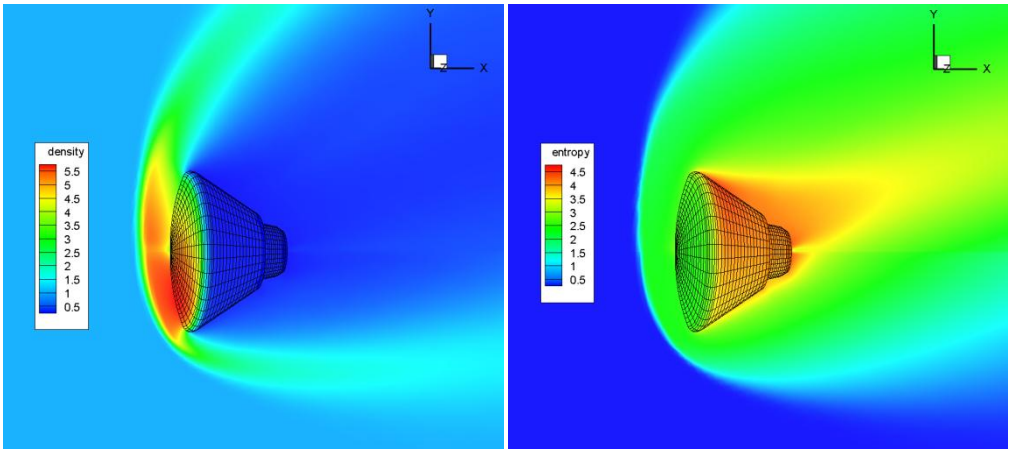

Figure 14: Density and entropy distributions around ARD
(Mach number=10, flow angle= -20°)

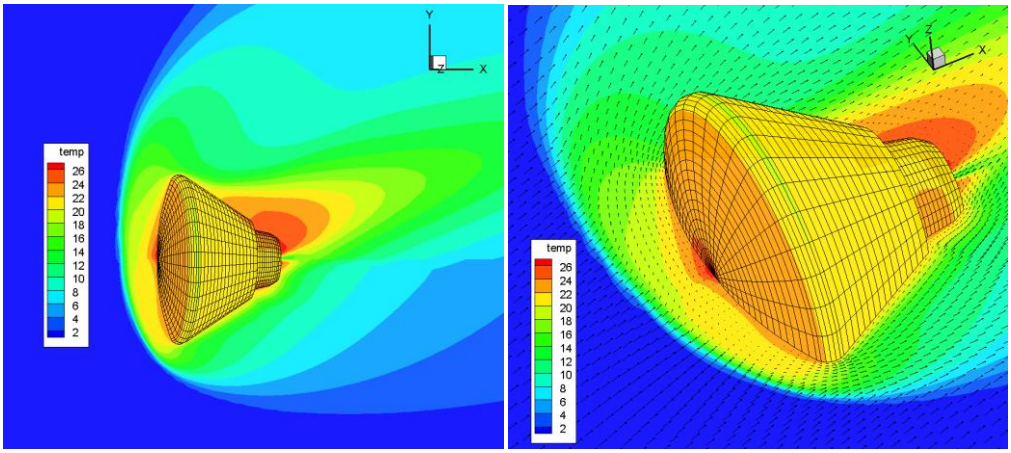

Figure 15: Temperature distributions and velocity vectors around Apollo AS-202
(Mach number=10, flow angle= -20°)

Flux vectors and streamlines at behind of ARD when angle of attack is -20° can be seen below. Vorticity appears at the top region after flow seperated from the geometry.

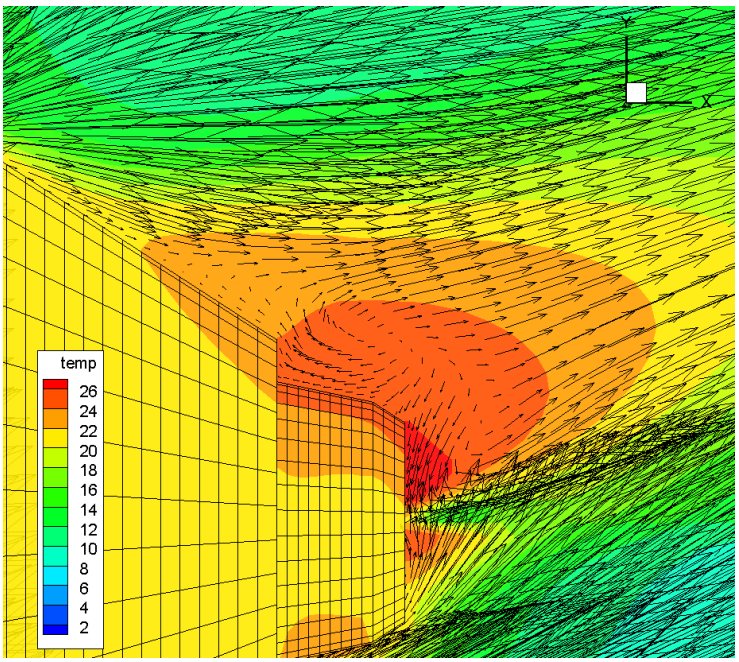

Figure 16: Flux vectors at the back region of ARD
(Mach number =10, flow angle = -20°)

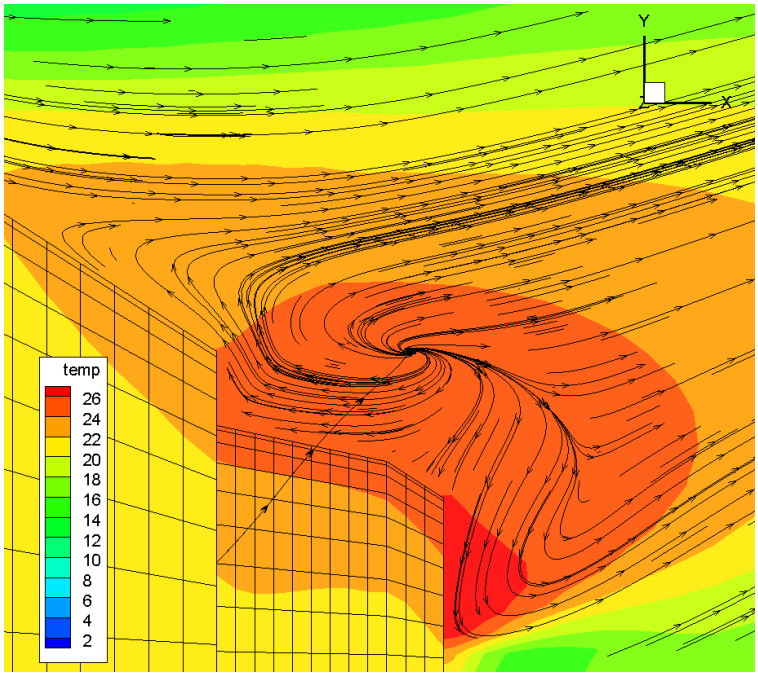

Figure 17: Streamlines at the back region of ARD
(Mach number =10, flow angle = -20°)

The Baldwin-Lomax turbulence model was implemented to the code and flow around ARD vehicle is examined when Mach number is 10 and angle between flow direction and x-axis is 0°. Some obtained results are seen in figure-18,19 and 20. Numerical values on figures are normalized.

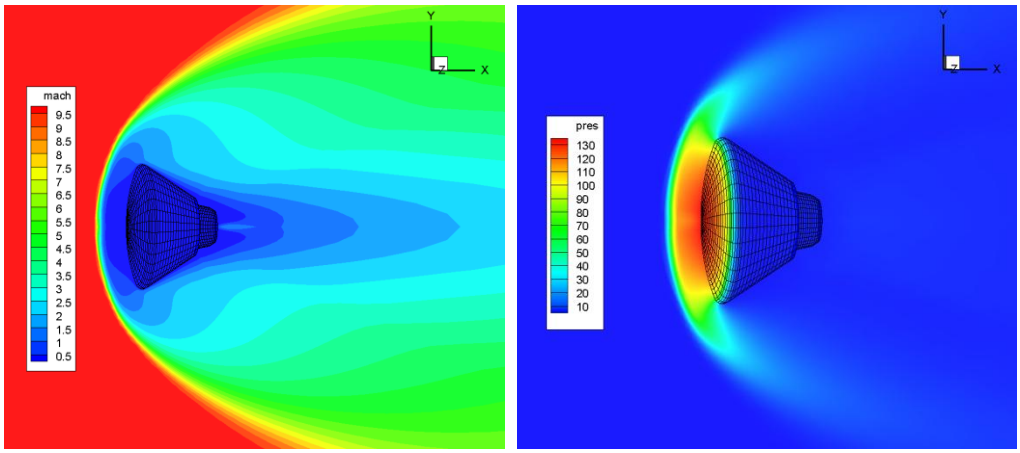

Figure 18: Mach number and pressure distributions around ARD
(Mach number=10, flow angle= 0°)

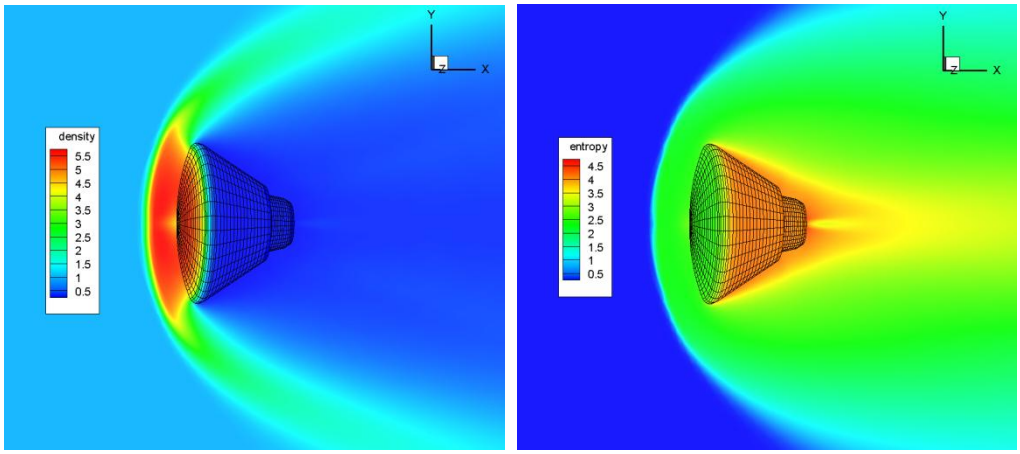

Figure 19: Density and entropy distributions around ARD
(Mach number=10, flow angle= 0°)

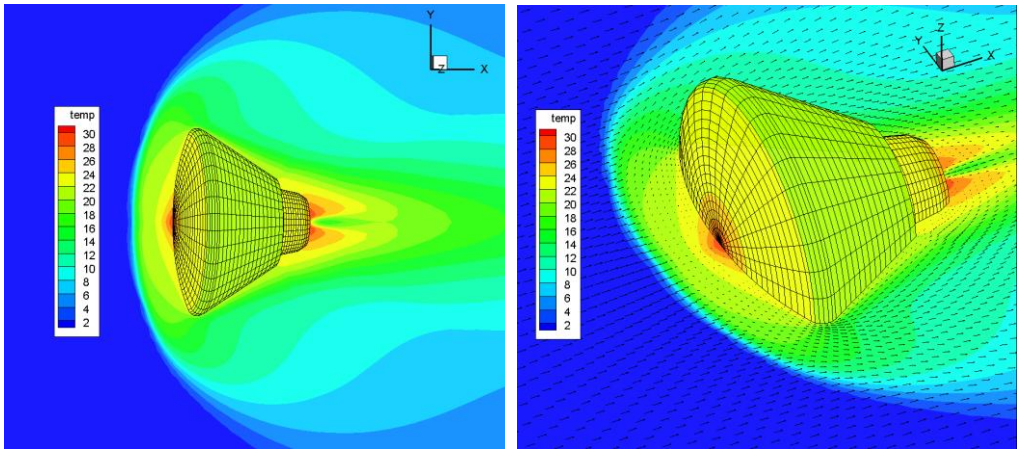

Figure 20: Temperature distributions and velocity vectors around Apollo AS-202
(Mach number=10, flow angle= 0°)

Streamlines and vorticity region at behind of ARD when angle of attack is 0° is seen in figure-21.

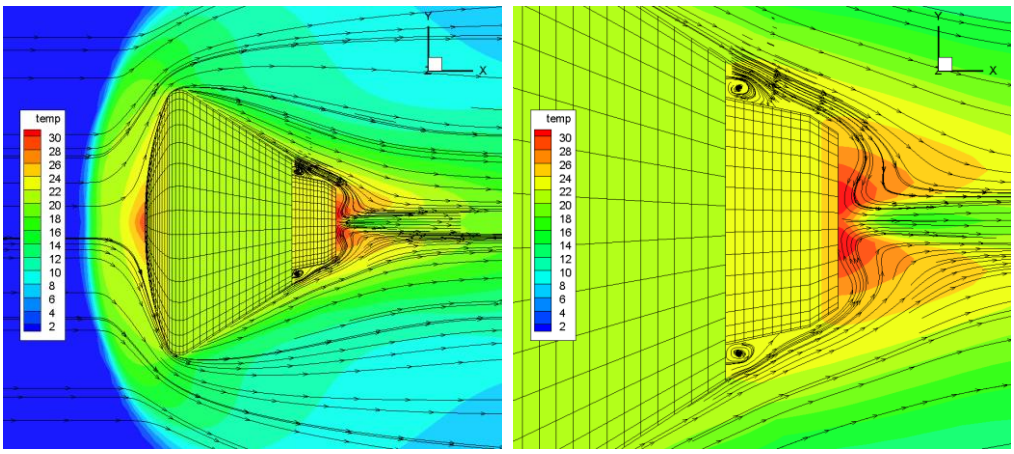

Figure 21: Streamlines and vorticity region around ARD
(Mach number =10, flow angle = 0°)

When results are inspected, it is seen that distributions of variables around ARD are generally like they are desired.

3 Conclusion and Future Work

The Navier-Stokes equations are solved with the Newton/Newton-Gmres method. The flow parameters are analyzed and convective heat transfer is studied on Apollo AS-202 Command Module. In the hypersonic turbulent flow analyze Baldwin-Lomax model is used. Additionally, spalart-allmaras turbulence model will be implemented to the flow solver and similar results will be observed and compared.

References

[1] T. Coratekin, J. van Keuk, and J.Ballmann, ''Performance of Upwind Schemes and Turbulence Models in Hypersonic Flows'', AIAA Journal, Vol.42, No.5, 2004

[2] R. Paciorri, W. Dieudonne, G. Degrez, J.-M. Charbonnier, and H. Deconinck, ''Exploring the Validity of the Spalart–Allmaras Turbulence Model for Hypersonic Flows'', Journal of Spacecraft and Rockets, Vol. 35, No. 2, 1998

[3] L. C. Scalabrin, "Numerical Simulation of Weakly Ionized Hypersonic Flow Over Reentry Capsules", Dissertation Submitted in Partial Fulfillment of the Requirements for the Degree of Doctor of Philosophy in the University of Michigan, Aerospace Engineering, 2007

[4] A. B. Gorshkov, '' Heat Transfer - Mathematical Modelling, Numerical Methods and Information Technology'', ISBN 978-953-307-550-1, 2011

[5] C. J. Roy, F. G. Blottner, '' Review and Assessment of Turbulence Models for Hypersonic Flows'', Progress in Aerospace Sciences, 42 (2006) 469-530, 2006

[6] R.H.Nichols, "Turbulence Models and Their Application to Complex Flows", University of Alabama at Birmingham

[7] C. J. Roy, F.G. Blottner, '' Methodology for Turbulence Model Validation: Application to Hypersonic Flows'', Journal of Spacecraft and Rockets, Vol.40, No.3, 2003

[8] L. Walpot, "Numerical Analysis of the ARD Capsule in S4 Wind Tunnel", 4th Europe Symposium of Aerothermodynamics for Space Applications, 2001, Capua,Italy

[9] J. J. Bertin, R.M. Cummings, (2009) "Aerodynamics for Engineers", ISBN-13: 978-0-13-235521-6, 2009